

Received September 17, 2019, accepted September 30, 2019, date of publication October 2, 2019, date of current version October 17, 2019.

Digital Object Identifier 10.1109/ACCESS.2019.2945119

High Refractive Index Metamaterials by Using Higher Order Modes Resonances of Hollow Cylindrical Nanostructure in Visible Region

XUFENG JING^{1,2,3}, YINUO XU^{1,2,3}, HAIYONG GAN³, YINGWEI HE³, AND ZHI HONG²

¹Institute of Optoelectronic Technology, China Jiliang University, Hangzhou 310018, China

²Centre for THz Research, China Jiliang University, Hangzhou 310018, China

³National Institute of Metrology, Beijing 100013, China

Corresponding author: Haiyong Gan (ganhaiyong@nim.ac.cn)

This work was supported in part by the National Key Research and Development Project of China under Grant 2017YFF0206103, in part by the Natural Science Foundation of Zhejiang Province under Grant LY17F050009, and in part by the National Natural Science Foundation of China under Grant 61875159.

ABSTRACT In order to design optical metamaterials to surpass the limitation of unnaturally high refractive index in visible range, we propose the nanocylinders nanostructure with hexagonal close-packed arrangement to precisely control the electric and magnetic resonances, resulting in the manipulation of the effective index of metamaterials. By drastically increasing the strong capacitive coupling between nanocylinders and decreasing the diamagnetic effect with core-shell nanostructure, the unnaturally high refractive index of designed metamaterials can be achieved to be 10.5 in visible region. The diamagnetic effect of solid nanocylinders can be significantly suppressed by using the design strategy of hollow nanocylinders with higher order mode resonances, leading to great enhancement of the effective refractive index in broadband visible region. Expanding the refractive index into an unnaturally high positive region in visible range can complete the spectrum of attainable refractive index, and the high refractive index metamaterials can provide more design flexibility for nanophotonics.


INDEX TERMS Metamaterial, high refractive index.

I. INTRODUCTION

The artificially engineering metamaterials have been developed to realize the desired materials which are not obtained in naturally materials [1]–[4]. The effective refractive indices in metamaterials can be tunable by critically design of artificial atoms [5]–[7]. It is known that the negative refractive index metamaterials [8]–[11] and near-zero index metamaterials [12], [13] have been extensively studied in last dozen years. However, the unnaturally high refractive index metamaterials have been sparsely researched, especially, in optical frequency. Expanding the refractive index to an unnaturally high positive region can go beyond the limitation of substances found in nature. The unnaturally high refractive index metamaterials with various artificial atoms will fill up the spectrum of attainable refractive index, and they will provide more flexibility in device design, such as, metamaterial cloaking in transformation optics and slow

light devices. Also, the high refractive index metamaterials have important applications in high resolution imaging [14] and lithography [15], where the resolution is proportional to the refractive index. It is also important to realize compact optical circuits and small electromagnetic devices by using the ultrahigh refractive index metamaterials.

In order to obtain high refractive index metamaterials, Sievenpiper *et al.* [16] proposed that a parallel plate capacitor with subwavelength array could enhance the effective permittivity. But, the effective permeability was simultaneously reduced due to the diamagnetic effect, leading to slightly enhancement of the effective refractive index. Interestingly, Wood *et al.* [17] proposed a close packed array of metallic cubes, which revealed the diamagnetic effect was attributed to the induced current loops in cubes. Shin *et al.* [18] demonstrated that the diamagnetic effect can be decreased by reducing the volume enclosed by the induced surface currents through structured cubes. By using appropriate structured cube elements, a larger improvement of the effective refractive index of metamaterial can be obtained with increasing

The associate editor coordinating the review of this manuscript and approving it for publication was Ildiko Peter .

the effective permittivity by the capacitive coupling effect and increasing the effective permeability by decreasing the diamagnetic effect. Recently, Choi *et al.* [19] proposed an “I”-shaped terahertz (THz) metamaterial with an unnaturally high refractive index by strongly coupled unit cells.

Although some achievements on the development of high refractive index metamaterials have been made, most of designed metamaterials focus on high effective refractive index in microwave, terahertz, or far infrared frequency ranges [16]–[25]. Owing to the difficulty of patterning nanoscale metalodielectric structures, there are few reports of optical metamaterials with unnaturally high refractive index in visible regime, hindering further practical applications. Going beyond the limit that is attainable with naturally existing substances and enlarging the possible range of indices in visible regime can lead to much improved performance of existing devices as well as the emergence of novel optical devices. If one can realize metamaterials with a high refractive index for visible wavelengths, it would be natural to expect diverse practical applications, such as super-resolution imaging, immersion lenses for lithography, compact optical modulators, and solar energy converters. Also, expanding the refractive index into a high positive regime will complete the spectrum of achievable refractive index and provide more design flexibility for transformation optics. Therefore, it is extremely important to develop metamaterials with ultra-high refractive index in the visible light range. We will demonstrate one kind of metamaterial to realize the effective refractive index as high as possible by using novel nanostructures with higher order resonant modes.

In this paper, a periodic nanostructure metamaterial with unnaturally high refractive index was designed by increasing the effective permittivity and reducing the current loop area to decrease the diamagnetic effect. We propose the cylinder nanostructure to implement this strategy. The obtained high refractive index in the broadband optical domain can be extended into the visible light region, which goes beyond the limitation of naturally achievable materials. By optimizing the geometric parameters, the effective permittivity and the effective permeability can be effectively controlled, leading to the manipulation of the unnaturally high refractive index.

II. PRINCIPLE OF HIGH REFRACTIVE INDEX

According to the effective refractive index $n = \sqrt{\varepsilon_r \mu_r}$, the index of metamaterials should be determined by the effective permittivity and the effective permeability. In order to maximize the effective refractive index, the effective permittivity ($\varepsilon = 1 + P/\varepsilon_0 E$) should be maximized, where P is the polarization and ε_0 is the permittivity in free space. Simultaneously, the effective permeability ($\mu = 1 + M/H$) should be increased, which can be achieved by the suppression of the diamagnetic effect as far as possible. M indicates magnetization. Generally, the effective permittivity can be increased by using the parallel plate capacitors which can be formed through the opposing faces of nearest neighbor sub-wavelength elements. When an electromagnetic wave with

the electric field vector perpendicular to the parallel plate element is applied, the formed capacitor will generate the accumulation effect of larger charges in gaps. Especially, the dipolar interaction between capacitors can also influence the polarization. Then, these charges in gaps can lead to a substantial dipole moment and the enhanced effective permittivity. But, these capacitors with larger volume show frequently strong diamagnetic response, which results in the decrease of effective permeability. So, the effective refractive index can not be greatly enhanced. Shin *et al.* [18] demonstrated that the diamagnetic effect resulted from the magnetic moments reduced by surface currents, and the strength of magnetic dipole moment was proportional to the area subtended by the current loops. Also, the diamagnetic response can be accurately controlled by the ratio of skin depth to the thickness of nanostructure [26], [27]. Therefore, the effective refractive index of metamaterials should be dependent on the different aspects of geometric structure.

Recently, Choi *et al.* proposed that the effective refractive index of designed metamaterials can be effectively evaluated by a parallel line charge accumulation model [19]. When the gap width g between metallic unit cells is far less than the size of unit cell of metamaterial, $g \ll L$, the strong coupled region is formed. It is found that the accumulated charges can be expressed by

$$Q \propto \varepsilon_0 \varepsilon_p \frac{L^3}{g} E_{in}, \quad (1)$$

where ε_p is the relative permittivity of the substrate material, and E_{in} indicates the incident electric field. For $g \leq L$ as the weakly coupled region, the accumulated charges in gaps can be represented as

$$Q \propto \varepsilon_0 \varepsilon_p (L - g)^2 E_{in}. \quad (2)$$

Then, the polarization density P can be calculated by

$$P = \frac{Q(L - g)}{L^2 d}. \quad (3)$$

Here, d is the physical thickness of unit cell of metamaterial. The effective permittivity of metamaterials can be evaluated by

$$\varepsilon_r = \varepsilon_p + \frac{P}{\varepsilon_0 E}. \quad (4)$$

In Eq.(4), $E = (L/g)^\beta E_{in}$, where β is a dimensionless fitting parameter. According to Eq.(1), it can be found that the decreased gap width will lead to the increase of the accumulated charges. Furthermore, the larger dipole moment resulting from the accumulated charges can increase the effective permittivity of metamaterials. Therefore, the empirical asymptotic formula to the effective refractive index can be obtained with the assumption of effective permeability being unity as [19]

$$n \cong n_p \left\{ 1 + \frac{\pi \alpha L}{2\sqrt{2}d} \left(1 - \frac{g}{L}\right)^3 + \frac{\pi \alpha \beta L}{2\sqrt{2}d} \left(1 - \frac{g}{L}\right)^4 \right\} \quad (5)$$

(in the weakly coupled regime),

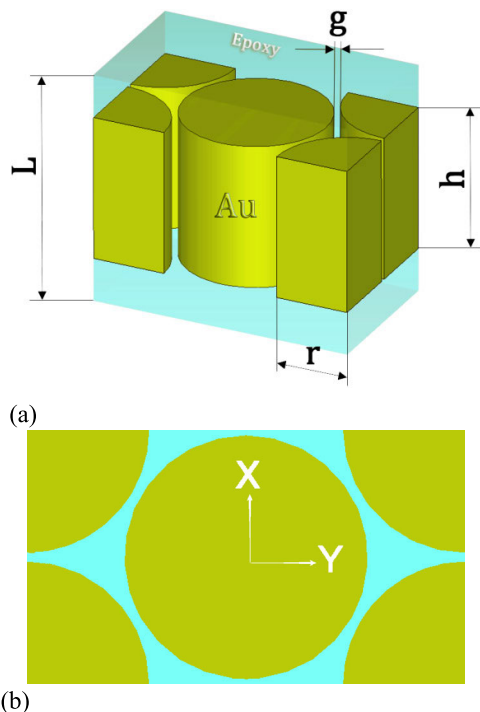


FIGURE 1. (a) One unit cell of nano-cylindrical structure metamaterial with gold material, (b) Top view of metamaterial structure with the arrangement of hexagonal two-dimensional periodicity.

$$n \propto n_p \alpha^{1/2} d^{-1/2} L^{(2-\beta)/2} g^{-(1-\beta)/2} \quad (6)$$

(in the strongly coupled regime),

where α is another dimensionless fitting parameter. Therefore, an ultrahigh index of refraction of metamaterial can be realized by further decreasing the gap width.

To realize an unnaturally high refractive index, specially, in visible light region, we should carefully design a nanostructure with sub-100nm artificial meta-atoms to control the polarization and magnetization, resulting in the maintenance of strong capacitive response and the suppression of the diamagnetic effect in metamaterials.

III. CYLINDRICAL PERIODIC NANOSTRUCTURE AS THE HIGH INDEX METAMATERIAL

From the principle of high refractive index metamaterials, it is known that the effect of the plate capacitor with changing gap width can be applied to increase the effective refractive index of metamaterials, and the polarization and magnetization can be adjusted by using geometric parameters. Here, we propose a nano-cylindrical structure metamaterial with gold material. Nanocylinders are arranged in the form of two-dimensional hexagonal periodicity. A single layer of gold nanocylinders is embedded in the dielectric material of epoxy ($n = 1.48$). In Fig.1, it is assumed that the complex permittivity of the gold cylinder particles used here follows the Drude model. The gold cylinder with height h and radius r is embedded in a base of epoxy resin material with height L , and g is the

gap between two adjacent gold cylinders. The period of the structure in the x direction and the y direction is $2 \times (r + g/2)$ and $2 \times 1.732 \times (r + g/2)$, respectively.

By using the finite integral method, the optical characteristics of the nanostructure metamaterial can be calculated, especially, in the visible region. All results reported in this paper were numerically calculated by the retrieval of effective parameter with S -parameter extraction method [28]–[32] combined with the numerical simulation of scattering parameters. All numerical simulations including transmission coefficients, reflection coefficients, phases, and electromagnetic field distributions were performed by using the commercial software Computer Simulation Technology (CST) Microwave Studio [33]. For the design of unit elements, an unit cell boundary condition was employed in an array configuration. For simplicity, the periodic boundary conditions were used for x and y directions. The perfect matched layer (PML), i.e., the open boundary condition, was used in z -direction. In simulations, the adaptive tetrahedral mesh refinement was used to obtain accurate mesh generation, and the grid spacing can be automatically given. This mesh refinement method in CST Microwave Studio has been used to accurately simulate nanoscale optical antennas [34] or graphene layer [35], [36] with the minimum mesh resolution achieving to 1nm. Thus, the accuracy is high enough to distinguish the nanoscale gap between nanocylinders in our simulations.

Originally, after optimization of structure parameters, we can define that the height of the gold cylinder is $h = 50\text{nm}$, the thickness of the entire substrate is $L = 80\text{nm}$, the radius of the cylindrical unit is $r = 25\text{nm}$. As the metal nanoparticles are inherently capped by 1nm thick organic ligand [37], [38], the minimal gap between nanocylinders here was set to be $g = 2\text{nm}$. When the incident light is incident on the nanostructure, the gap between adjacent two cylinders is equivalent to a capacitor, and a large amount of charges converge on the side surface of the nanocylinders. This kind of extreme charge distribution results in the formation of dipoles at the edges of the metal cylinder and an increase of the effective permittivity. The strength of capacitive coupling is dependent on the interface area between adjacent cylinders.

Another key factor to realize ultrahigh refractive index results from the suppression of the diamagnetic effect [20], [39]–[50]. Magnetically induced anti-resonance is evident, and the shape of the unit cell maybe affects this response. The hexagonal close-packed cylinders can reduce the volume subtended by induced current loops, resulting in the reduction of the current loop density [50]. This kind of arrangement of nanocylinders can efficiently suppress the diamagnetic effect, so that the magnetic permeability maintains a relatively high value in a specific region. Therefore, in order to obtain the high refractive index of metamaterials, the nanostructure should be carefully designed to enhance the effective permittivity and permeability.

IV. RESULTS OF HIGH REFRACTIVE INDEX METAMATERIALS

On basis of S -parameter extraction method [28]–[32], we firstly extracted the effective permittivity of metamaterial as shown in Fig.2(a). It can be seen that the effective dielectric constant exhibits a lower frequency fundamental mode and a higher second-order mode in the near-infrared band. The effective dielectric constant at the fundamental mode frequency is as high as 324, and the peak value in the second-order mode is 76. According to the Mie theory for nanoparticles, the coupling of the incident light with normal modes of nanoparticles strongly depends on the mode number and size parameters [39]. Because higher modes feature the distance between any two adjoining poles in the field patterns that decreases with the mode number, the coupling with higher-order modes is less effective [40]. Thus, the mainly fundamental dipolar normal mode can be excited when the size of nanoparticles is much smaller than the incident wavelength. However, as the size of nanoparticles increases, the contribution of higher-order modes becomes larger and can no longer be ignored. So, the scattering induced by higher order modes with larger nanoparticles play a major role. In other words, the higher order modes become comparable and may dominate the scattering with increasing incidence frequency. In our designed nanocylinders with $r = 25\text{nm}$ and $h = 50\text{nm}$, the fundamental resonant mode occurs at the incident wavelength of about 1300nm, and the second-order resonant mode is at about 880nm of incident wavelength as shown in Fig.2(a).

Magnetic permeability control is another key factor to increase the refractive index. In Fig.2(b), it can be seen for the effective permeability that there are smaller values at the resonant region, but the higher resonant peaks for the effective permittivity occur at same frequencies in Fig.2(a). This may be attributed to the diamagnetic effect in infrared range. The occurrence of diamagnetic response causes a decrease in magnetic permeability. At the first order resonant position at the wavelength of about 1300nm, the magnetic permeability is near zero. In Fig.2(b), the blue arrow at the wavelength of 1300nm shows the fundamental resonant mode, and the blue arrow at the wavelength of about 870nm indicates the second-order resonant mode. It is interesting that at the second order resonance the real part of magnetic permeability can achieve to be 4. The peak of magnetic permeability in visible region can reach to be 12 in more higher order resonance. Thus, our proposed metamaterial nanostructure can enhance the magnetic permeability in higher order resonances, leading to the increase of the effective refractive index in visible region.

The corresponding effective refractive index of metamaterial was calculated in Fig.2(c). An unnaturally high refractive index in the visible light region (400 to 760 nm) is revealed. The peak of index can reach to be 10.5, which is difficult to achieve in nature material. Although the effective permittivity at 760nm for the second-order resonant mode is lower relative to that of the fundamental mode, the peak of refractive index

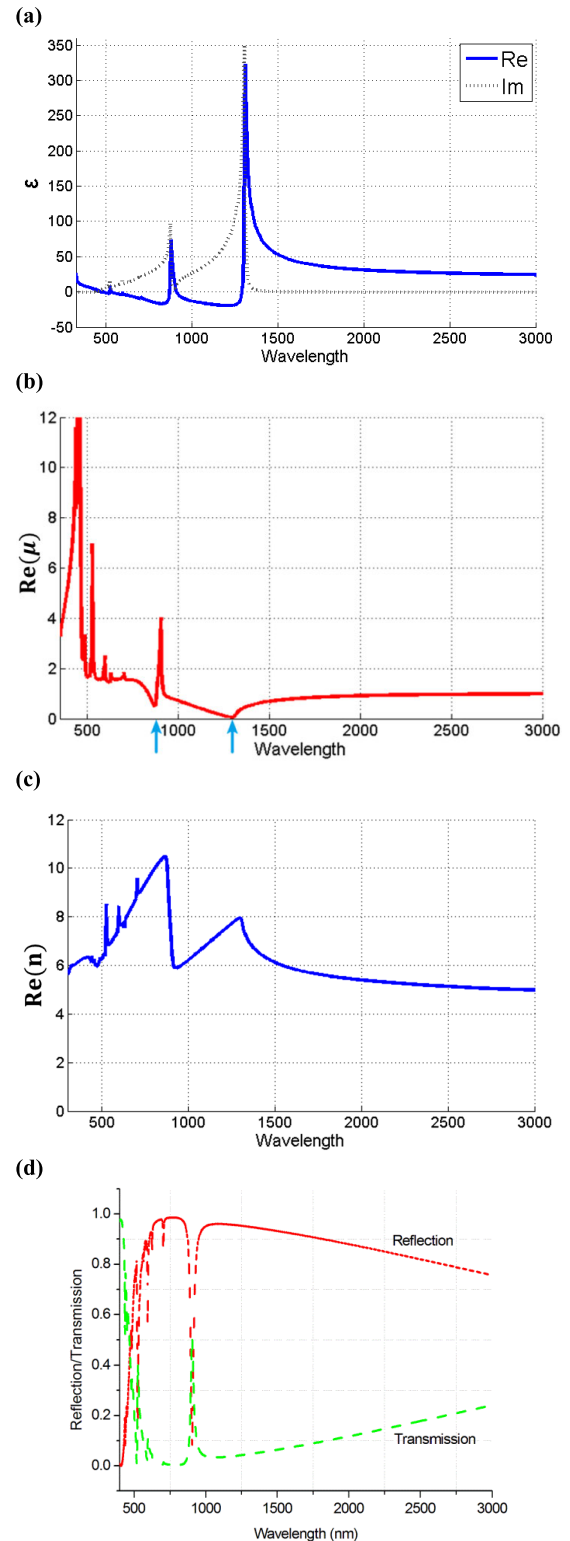


FIGURE 2. (a) Numerically calculated effective permittivity of nanocylinder metamaterial, (b) the real part of the effective permeability, (c) the real part of the effective refractive index. (d) The corresponding reflection and transmission.

of the structure is the highest ($\text{Re}(n) = 10.5$) due to the decrease of the diamagnetic effect. It should be noted that there are some sharp resonant peaks of the effective index in

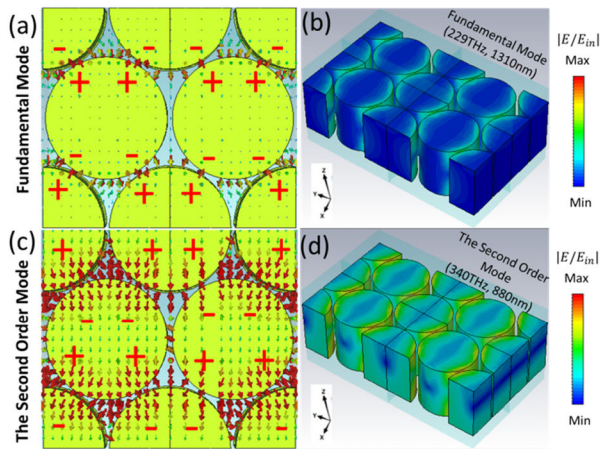


FIGURE 3. (a) Top view of the electric field distribution at the fundamental mode resonant frequency, (b) Spatial distribution of the electric field at the fundamental resonant mode, (c) Top view of the electric field distribution at the second order resonant mode, (d) Spatial distribution of the electric field at the second order resonant mode.

visible region, which can be ascribed to higher order magnetic resonances. In Fig.2(d), the corresponding reflection and transmittance are shown.

In order to reveal the physical nature of the high refractive index, we calculated the electromagnetic field distribution of nanostructure at resonant frequencies. Figure 3(a) shows the top view of the electric field distribution at the fundamental mode resonant frequency of 229THz. The strongly confined electric field is distributed in the gaps between nanocylinders. It can be seen that a larger amount of charges are accumulated at each edge of the faced nanocylinders, leading to the generation of the huge dipole moment in the gaps between nanocylinders. According to the capacitive effect of parallel plate, it should be noted that the direction of confined strongly electric field vector is inverse to that of incident field. The intensity of electric field in the gap at the electric resonance is much stronger than that of incident field, which leads to the enhancement of the effective permittivity. Also, the spatial distribution of the electric field intensity at the fundamental mode is shown in Fig.3(b). In Fig.3(c), it is demonstrated that the electric field distribution for the second order mode at the resonant frequency is revealed. The huge dipole moment is generated in the gaps of nanocylinders. The strength of the confined electric field at the second order mode is much stronger than that at the fundamental resonant mode. Such confined electric field at the second order mode can deeply penetrate into the depth of the gaps of nanocylinders. The spatial distribution of the saturated electric field at the electric resonance wavelength for the second order mode is also observed in Fig.3(d).

Another key factor to improve the effective refractive index of designed metamaterial is to suppress the magnetic diamagnetic effect of nanostructure. We should make the diamagnetic effect as small as possible. As shown in Fig.2(b), there is the real part of the effective permeability. It can be seen that the magnetic anti-resonances at the fundamental mode

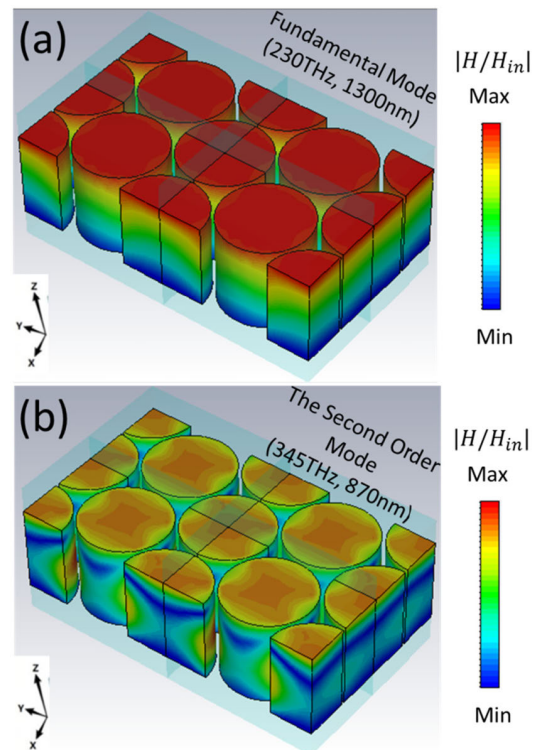


FIGURE 4. Spatial distribution of saturation magnetic field at (a) the fundamental resonant mode and (b) the second order resonant mode, respectively.

and the second order mode are demonstrated, which can be verified by $d\mu/d\lambda$ opposite to $d\varepsilon/d\lambda$. At the dips of the magnetic permeability, there are the indicators of the diamagnetic response. The fundamental mode of the anti-resonance response indicates a significantly diamagnetic effect with the dip of $\text{Re}(\mu)$ (near to zero) at the wavelength of 1300nm. The diamagnetic response at the second order mode is revealed with $\text{Re}(\mu) = 0.6$ at the wavelength of 870nm. In order to confirm this diamagnetic response, the spatial distribution of saturated magnetic field intensity was calculated at the fundamental mode and the second order mode at the resonant frequencies, respectively, as shown in Fig.4. Figure 4(a) shows the spatial distribution of saturated magnetic field at the fundamental resonant mode of 230THz. The significant diamagnetic response can be confirmed by the suppressed penetration of magnetic field. In Fig.4(b), the spatial distribution of saturated magnetic field at the second order resonant mode of 345THz is revealed. Compared with the fundamental mode, the increased penetration depth ($\sim 50\text{nm}$) of magnetic field for the second order mode reveal the suppression of diamagnetic effect. It is interesting that the higher order resonant modes can effectively suppress the diamagnetic response, specially, in visible region.

V. THE INFLUENCE OF MULTIPLE PARAMETERS ON REFRACTIVE INDEX

In order to show the influence of the geometrical parameters of the cylindrical structure on the effective refractive index,

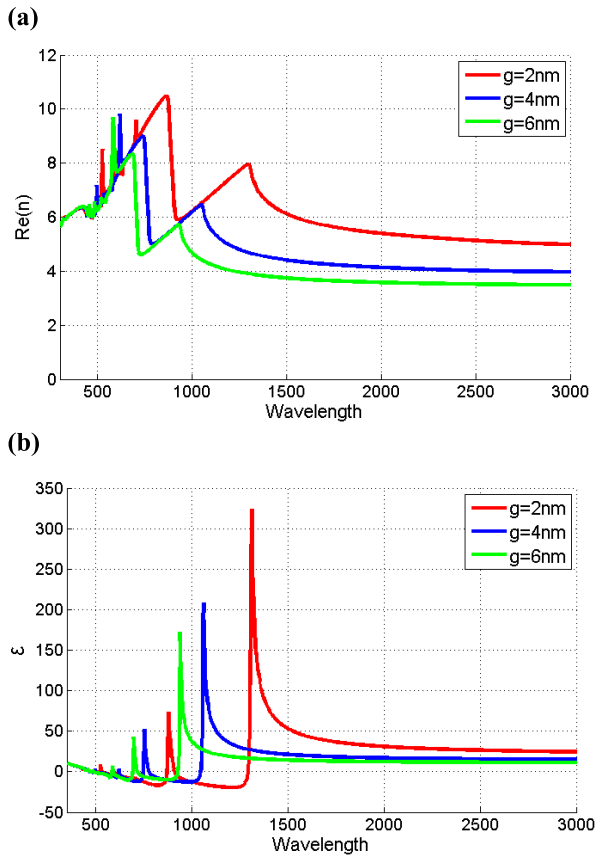


FIGURE 5. (a) The real part of effective refractive index with changing gap g . (b) The real part of effective permittivity with changing gap g .

we will demonstrate the characteristics of the index with changing the gap g , the height h , the radius r and the shape of the structure element.

A. EFFECT OF GAP G ON REFRACTIVE INDEX

Figure 5 shows the performance of the effective index with changing the gap g . For the unit cell of metamaterial, other parameters are unchanged with $h = 50\text{nm}$ and $r = 25\text{nm}$. As the gap between cylinders increases, the resonant peak of the effective index shifts toward the short wave direction in Fig.5(a). It is noted that for $g = 4\text{nm}$ the second order resonance mode with the peak of high refractive index move to visible region. The value of the sharp peak for more higher order resonant mode is higher than that for the second order mode. The largest value of high refractive index can reach to near 10 in the visible region. For $g = 6\text{nm}$, the resonant peak of high refractive index continue to be of blueshift. But, the peak of index is slightly decreased. The similar variability of the effective permittivity is shown in Fig.5(b). The value of the effective permittivity at the peak frequencies is significantly reduced. This means that the equivalent parallel plate coupling is weakened, and a large amount of charges escape from the cylinder gap. The electrical response strength is also reduced, and the refractive index is lowered.

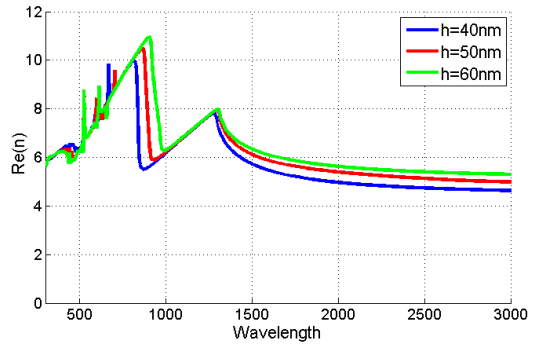


FIGURE 6. Effect of cylinder height on refractive index.

B. EFFECT OF CYLINDER HEIGHT H ON REFRACTIVE INDEX

Figure 6 shows the real part of index with different heights of nanocylinders. Here, the gap between adjacent cylinders is always 2 nm, and the radius of each cylinder is 25 nm. As the height of the Au cylinder increases, the volume of the structure gradually increases, and it becomes difficult for free electrons to penetrate into the dielectric layer. But, the electric resonance is enhanced as the height increases, leading to the improvement of the effective index in the second order mode. As the height h becomes larger, the free electrons trapped between the cell gaps are thus increased, so that the equivalent capacitive coupling is enhanced, causing a stronger electrical resonance. Therefore, to a certain extent, the increase of the height h of the cylinder can increase the refractive index of the structure. Although the diamagnetic response increases, the electric resonance with dipole moment is also enhanced as the height increases, resulting in the improvement of index. Thus, the manipulation of the effective permittivity and permeability is competitive process, and the highest effective refractive index of metamaterials can be obtained by using the optimum structural parameters.

C. EFFECT OF CYLINDRICAL RADIUS R ON REFRACTIVE INDEX

Next, the influence of the radius r of the cylinder on the refractive index is analyzed. Here, the height of the cylinder is always 50 nm, and the gap between the cylinders is 2 nm. In Fig.7, increasing the radius of the cylinder to a certain extent is beneficial to concentrate the charges to the gap to enhance the electrical response. When the radius is too large, the area occupied by the specified gap size within the unit area will reduce the electrical resonance, leading to the decrease of the refractive index. Therefore, a suitable radius r is an important factor in obtaining a higher effective refractive index.

D. EFFECT OF SPECIFIC SHAPE OF NANOSTRUCTURE ON REFRACTIVE INDEX

The above research is based on the hexagonal periodic arrangement of the cylinder to study the refractive index, but the influence of the geometric shape on the refractive

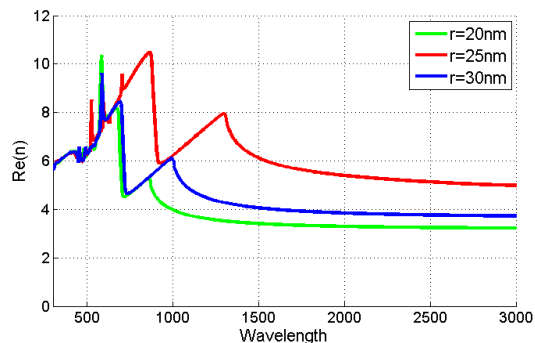


FIGURE 7. Effect of cylindrical radius on refractive index.

index is also critical. Here, we discuss the geometric three-dimensional particles as the gold cubes on the effective refractive index in Fig.8. The length, width and height of the cubes are set to be $a = 50\text{nm}$, the thickness of the entire substrate is $L = 80\text{nm}$, and the gap between the cubes is 2nm as shown in Fig.9(a).

The effective permittivity of cubes was calculated as shown in Fig.8(a). Compared with the effective permittivity in Fig.2(a) for nanocylinders, the effective permittivity is enhanced for nanocubes at the fundamental mode resonance with the value of more 500. The effective permittivity is also increased slightly for the second order resonant mode. This changed geometrical shape to enhance the effective permittivity can be attributed to the improved capacitive coupling effect between nanoparticles as shown in Fig.9(b). When the electromagnetic wave is incident on the array of nanocubes, the oppositely different charges are accumulated at the faces of each paired nanoparticles at the resonant frequency of capacitive coupling. This can result in huge dipole moment within the gaps of nanocubes. The capacitive coupling between nanocubes can excite the large polarization density, resulting in the enhancement of the effective permittivity. The strength of this capacitive coupling mainly depends on the interfacial area between adjacent nanoparticles. For nanocubes, the area of surface contact with 250nm^2 is advantageous over the nanocylinders with the hook face contact, leading to the increase of the effective permittivity. The accumulated charges at each edge of the faced nanocubes with the capacitive coupling also can be revealed in the spatial distribution of the saturated electric field at the resonant modes as shown in Fig.9(c) and Fig.9(d). The strongly confined electric field across the gaps reveals the huge dipole moment. Compared with the distribution of electric field in Fig.3 for nanocylinders, the strength of the confined electric field for nanocubes is stronger than that of nanocylinders, confirming the improvement of the effective permittivity at the resonant modes.

Figure 8(b) shows the numerically retrieved real part of permeability for nanocubes. The magnetic anti-resonance is obvious, and the dips of $\text{Re}(\mu)$ are the indicators of the diamagnetic effect. It is known that the diamagnetic response is mainly determined by the volume subtended

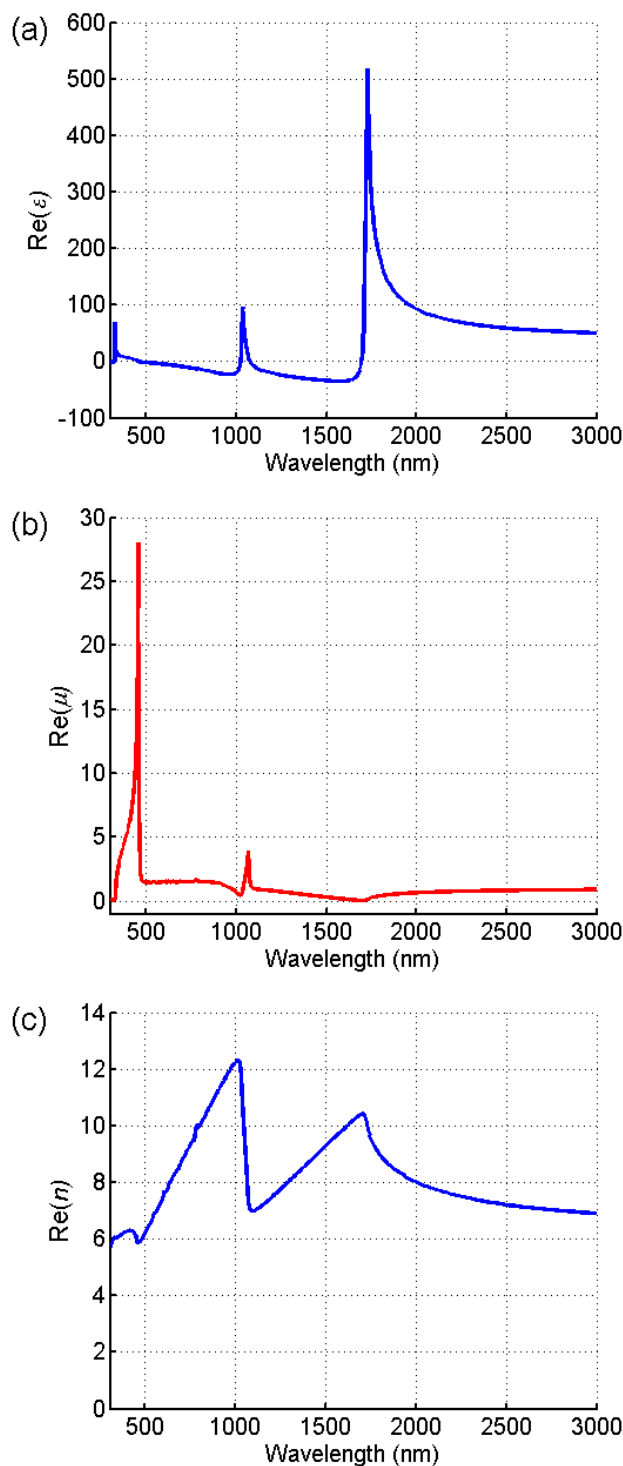


FIGURE 8. (a) Numerically calculated effective permittivity of nanocubes, (b) the real part of the effective permeability of nanocubes, (c) the real part of the effective refractive index of nanocubes.

by the current loops perpendicular to the incident magnetizing field. Compared with the effective permeability of nanocylinders in Fig.2(b), the nanocubes lead to a stronger diamagnetic effect, as confirmed by the lowest dip of $\text{Re}(\mu)$ in Fig.8(b) and the calculated volume of single nanocube subtended by the current loops. The diamagnetic response is

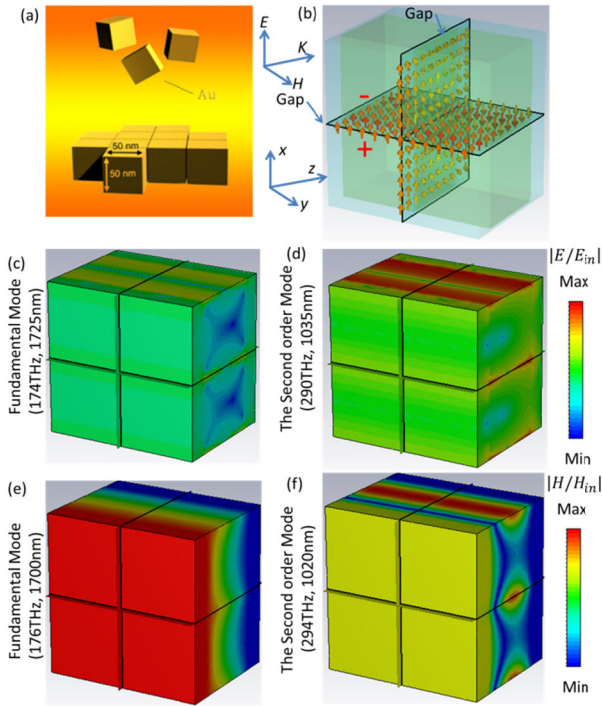


FIGURE 9. (a) Schematic for the assembly of nanocubes, (b) the electric field distribution at the fundamental mode resonant frequency of 174THz, (c) Spatial distribution of the saturated electric field at the fundamental resonant mode, (d) Spatial distribution of the saturated electric field at the second order resonant mode, (e) Spatial distribution of the saturated magnetic field at the fundamental resonant mode, (f) Spatial distribution of the saturated magnetic field at the second order resonant mode.

further confirmed by the suppressed penetration of magnetic field as shown in Fig.9(e) and Fig.9(f). Also, the direct comparison of spatial distribution of the saturated magnetic field for nanocubes with the nanocylinders in Fig.4 allows us to systematically figure out the effect of geometrical shape on the diamagnetic effect. Even if the height of nanoparticles is same, the nanocylinders exhibit much suppressed diamagnetic effect due to less density of the current loops.

Figure 8(c) shows the numerically retrieved real part of refractive index for nanocubes. It can be seen that the refractive index is maximized at the wavelength of electric resonances. The peak index of more than 12 at the wavelength of 1000nm with the second order mode can be achieved. Compared with the effective index for nanocylinders in Fig.2(c), the obtained peak refractive indexes of nanocubes are obviously redshifted to maximize in infrared region. Also, the higher-order modes of high refractive index are conspicuously absent in visible region.

VI. CORE-SHELL COMBINED CYLINDRICAL METAMATERIAL ON HIGH REFRACTIVE INDEX

On basis of the principle of high refractive index metamaterial, the higher index can be realized by reducing the volume of metallic particles subtended by the current loops. Then, we propose the core-shell cylindrical structure as shown in Fig.10. The structure introduces some new freedom of

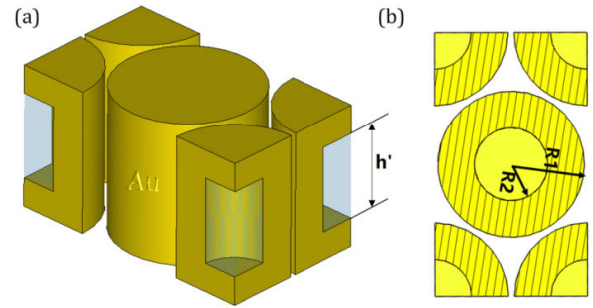


FIGURE 10. (a) Core-shell combined cylindrical nanostructure, (b) Top view of nanostructure.

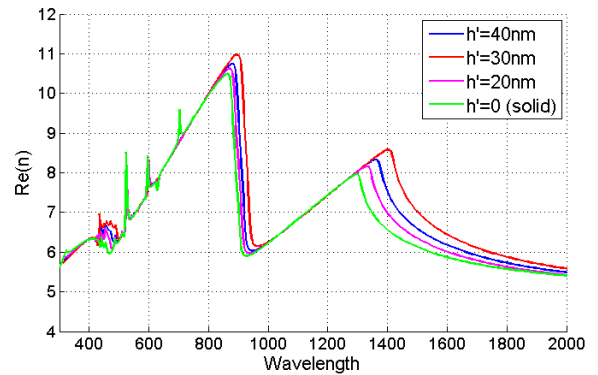


FIGURE 11. The real part of the effective refractive index for core-shell cylindrical nanostructure with filled air.

parameters to control the effective refractive index of metamaterials. The cylindrical outer radius is defined as $R1$, the cylindrical inner radius is defined as $R2$, and the height of cylindrical air core is defined as h' . The cylinders are also embedded into the substrate material of epoxy resin with $L = 80nm$. Figure 11 shows the real part of the effective refractive index as a function of the height of air core. Here, $R1=25nm$, $R2=12.5nm$, and $g = 2nm$. It can be seen that the index can achieve to be about 7.0 in the visible light region when $h' = 30nm$.

It is known that the strength of the magnetic dipole is proportional to the volume subtended by the current loops, and thus the diamagnetic response of the hollow structure is effectively reduced. The significant increase of magnetic permeability leads to an increase of the refractive index, especially, in visible region. The magnetic field strength distribution at 231 THz with $h' = 30nm$ is shown in Fig.12. Here, $R1=25nm$, $R2=12.5nm$, and $g = 2nm$. It can be seen that the penetration depth is obviously increased compared with that of the solid cylinders nanostructure, leading to the great suppression of diamagnetic effect.

Next, we replace the air core in cylinders by the silicon dioxide ($n = 1.54$) material with unchanged geometric parameters as shown in Fig.13. Here, $R1=25nm$, $R2=12.5nm$, and $g = 2nm$. The height of the core is $h' = 30nm$. In Fig.13(a), the Au cylindrical shell and epoxy matrix are treated with increased transparency to emphasize the silica material. In Fig.13(b) and (c), it is found that

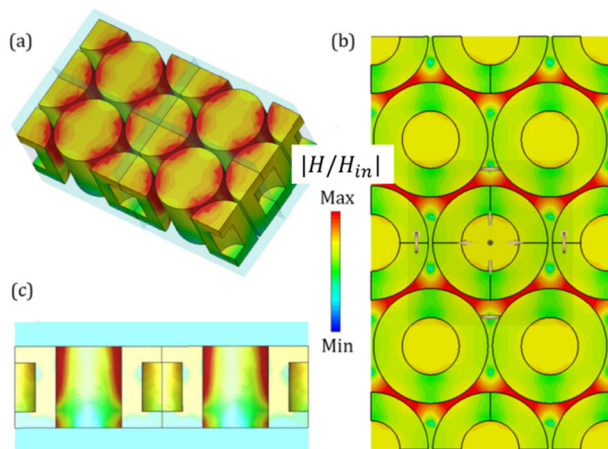


FIGURE 12. (a) Three-dimensional map of the magnetic field strength, (b) the magnetic field strength distribution in the *x-y* plane, (c) the magnetic field strength distribution in the *x-z* plane.

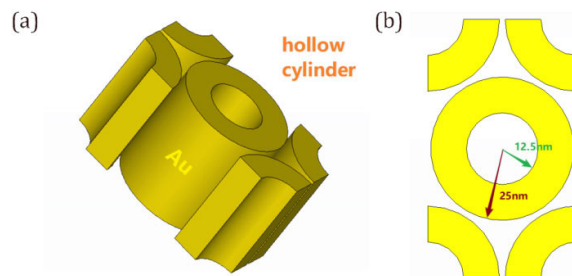


FIGURE 14. (a) Hollow cylindrical perspective view, (b) Top view of hollow cylindrical nanostructure.

demonstrated in Fig.15(b). These results may be attributed to the suppression of diamagnetic effect with the hollow cylinders. The metal volume of the hollow cylinders is smaller than that of the solid cylinders, so that the diamagnetic effect is also smaller, which in turn cause the refractive index to be larger.

In order to further disclose the physical origin of high refractive index for the hollow cylinders nanostructure metamaterial, the effective permittivity, the effective permeability, the electric field distribution, and the magnetic field distribution are respectively demonstrated in Fig.16 and Fig.17. In Fig.16(a), the effective permittivity of hollow cylinders is shown, and there is no significant difference of the amplitude of permittivity between the hollow cylinders and the solid cylinders. The obtained high effective permittivity is dependent on the capacitive coupling between nanocylinders at the resonant frequencies. The huge dipole moment with the large charges accumulated at the faces of each paired cylinders can be obtained within the gap of nanoparticles. The strength of the capacitive coupling is mainly dependent on the interfacial area between adjacent nanoparticles. Because the interfacial area between adjacent nanoparticles for the solid cylinders and the hollow cylinders is same, the amplitude of permittivity is similar at the resonant frequencies. Compared with the permittivity of the solid cylinders in Fig.2(a), the resonant frequencies for the fundamental mode and the second order mode are redshifted. According to the Mie theory for nanoparticles, the resonant frequencies are related with the size of nanoparticles [39], [40]. In other words, the resonant frequencies will be redshifted with the increased size of nanoparticles. For the hollow cylinders, the cores of cylinders are filled with the dielectric material, which is equivalent to increase the size of nanoparticles. Thus, the spectrum of resonant modes for the hollow cylinders in Fig.16(a) is slightly redshifted compared with that of the solid cylinders.

The extracted permeability for these two kind of nanostructures is distinctly different, specially, in visible region as shown in Fig.16(b). The maximum of $Re(\mu)$ can reach to be more than 20 at about 550nm for the hollow nanocylinders. It is known that the intensity of effective permeability of nanoparticles is related with the volume subtended by the current loops. For the hollow cylinders, it is obvious that the volume subtended by the current loops is smaller than that for the solid cylinders. So, the amplitude of the effective

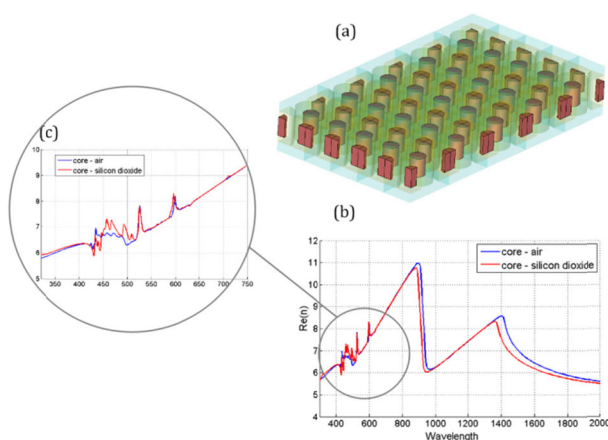


FIGURE 13. (a) Core-shell cylindrical nanostructure with the silicon dioxide material in core, (b) The real part of the effective refractive index with different core material, (c) The partial enlarged view of index in visible region.

the effective index of metamaterial in visible region can be increased by filling the high refractive index material into the core of nanocylinders. Therefore, the core-shell cylindrical metamaterial structure proposed in this paper can achieve high refractive index characteristics in the visible light region, and the peak value of the refractive index reaches to be more than 8.0.

Next, in order to realize the broadband high refractive index performance in the center frequency range of visible light from 450nm to 550nm, we propose the hollow cylindrical nanostructure metamaterial as shown in Fig.14. The hollow cylindrical nanostructure is embedded in epoxy resin. The geometric parameters are unchanged except for the inner radius 12.5nm of cylinders. The extracted refractive index of the hollow cylinders is shown in Fig.15. It can be seen that the broadband high refractive index can be achieved in visible region, specially, from 450nm to 550nm. The partial enlarged view of the real part of the effective refractive index for hollow cylinders and solid cylinders, respectively, is

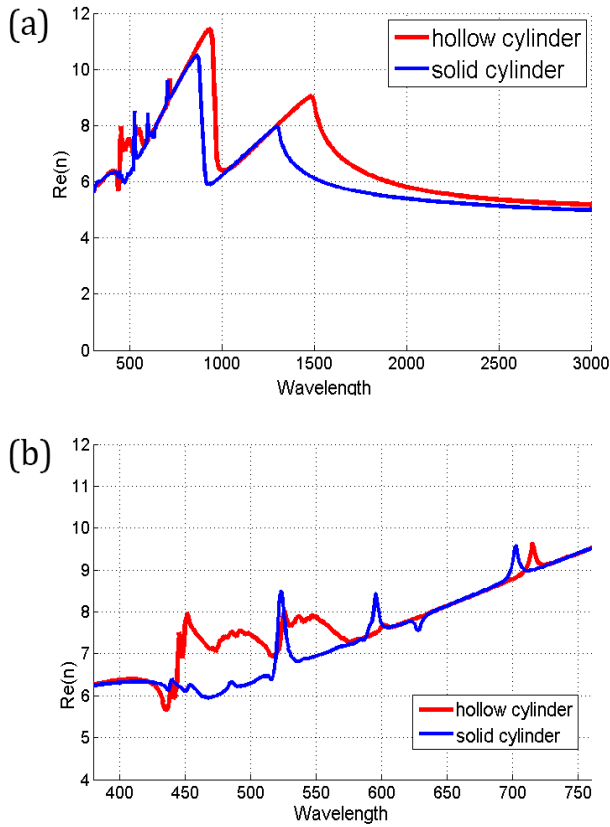


FIGURE 15. (a) The real part of the effective refractive index for hollow cylinders and solid cylinders, (b) The partial enlarged view of index in visible region.

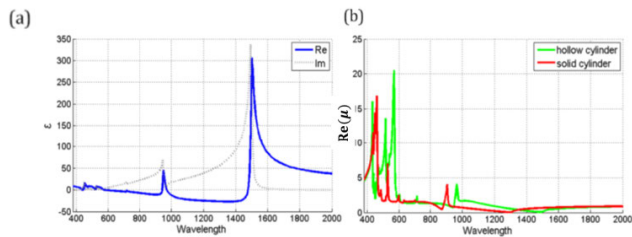


FIGURE 16. (a) Effective permittivity of hollow cylinder (b) Magnetic permeability of hollow cylinder and solid cylinder.

permeability for the hollow cylinders is higher than that of the solid cylinders, specially, in the visible region. Thus, the diamagnetic effect of solid cylinders can be significantly suppressed by the design of hollow cylinders, leading to the great enhancement of the effective index. In addition, the spectrum of the resonant frequencies for the hollow cylinders is clearly redshifted compared with that of the solid cylinders. This spectrum change of the effective permeability can be also attributed to the increase of the effective size of hollow cylinders nanoparticles according to the Mie theory.

In order to reveal the physical nature of high refractive index for the hollow cylinders, the spatial distributions of the saturated electric and magnetic field at the fundamental resonant mode and the second order mode are numerically demonstrated in Fig.17. Figure 17(a) shows the spatial distribution of the saturated electric field at the fundamental

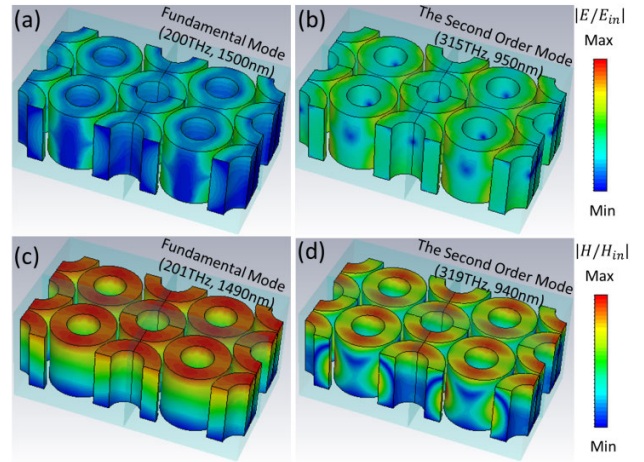


FIGURE 17. (a) Spatial distribution of the saturated electric field at the fundamental resonant mode, (b) Spatial distribution of the saturated electric field at the second order resonant mode, (c) Spatial distribution of the saturated magnetic field at the fundamental resonant mode, (d) Spatial distribution of the saturated magnetic field at the second order resonant mode.

TABLE 1. Performance comparison. The effective refractive index value of the current state of the art is compared with that of the reported structures.

References	Frequency /Wavelength	Value of Index	Structures
Ref.[41]	Relative wavelength	~4.0	Cut-through slits.
Ref.[42]	~100GHz	~5.5	Metallic gratings
Ref.[43]	12.43GHz	~20.9	The eight layers cut wires array
Ref.[18]	~70THz	~7.0	Metallic cubes
Ref.[44]	~850nm	~2.8	The stacked metallic cut-wire structures.
Ref.[19]	~0.85THz	~33.22	Five-layer “I”-shaped structure
Ref.[45]	1.55μm	~62.0	Deep-subwavelength optical waveguides
Ref.[46]	~0.51THz	~22.19	I-shaped silver electrodes
Ref.[47]	~1.5GHz	~3.91	Structured cubes
Ref.[48]	~0.315THz	~14.36	Z-shaped metamaterials
Ref.[49]	~2.14THz	~67.9	Four layers “I” shaped metallic patches
Ref.[20]	~2.11THz	~77.02	Metal-dielectric-metal checkboard structure
This work	~760nm	~10.5	Nanocylinders

resonant mode at the wavelength of 1500nm. Compared with the distribution of the electric field in Fig.17(a), the intensity is clearly enhanced in the gaps between hollow cylinders for

the second order resonant mode at the wavelength of 950nm. The charges can be accumulated at the each edge of the faced nanocylinders, and the dipole moment is generated in gaps, leading to the enhanced electric resonance. Figure 17(c) shows the spatial distribution of the saturated magnetic field at the fundamental resonant mode at the wavelength of 1490nm. Compared with the distribution of the magnetic field in Fig.17(c), the magnetic field at the second order resonant mode at the wavelength of 940nm can penetrate the whole hollow cylinders along the propagation direction in Fig.17(d). Thus, the diamagnetic effect of hollow cylinders nanostructure metamaterial can be efficiently suppressed by higher order resonant mode.

VII. CONCLUSION

Based on the principle of achieving high refractive index, the periodic nanostructure of cylindrical unit with high refractive index in the visible light region is designed. This structure is the hexagonal periodic arrangement of single-layer cylinders. The electromagnetic properties of the metamaterial are analyzed on the basis of the coupling of the capacitor to enhance the electrical response and the hexagonal arrangement to reduce the diamagnetic effect. By adjusting the geometric parameters of nanocylinders, such as the gap width, the height of cylinders, the radius of cylinders, and the shape of nanostructure, the effective permittivity and the effective permeability can be flexibly controlled. The peak of the effective index can achieve to be 10.5 at the wavelength of 760nm. It is interesting that the sharp peaks of high refractive index at the higher order resonant modes in the visible region can be obtained. In order to further suppress the diamagnetic response of cylinders, we propose the core-shell structure to achieve a further increase in refractive index. Importantly, in order to realize the broadband high refractive index in visible region, the hollow cylinders nanostructure metamaterial is designed. The maximum of $\text{Re}(\mu)$ can reach to be more than 20 at about 550nm. Thus, the diamagnetic effect of solid cylinders can be significantly suppressed by the design of hollow cylinders, leading to the great enhancement of the effective index. The maximum of the effective index can reach to be 8.0 at the center frequency range of visible light from 450nm to 550nm. Moreover, The effective refractive index value of the current state of the art is compared with that of the reported structures in Table 1.

REFERENCES

- [1] A. D. Neira, G. A. Wurtz, and A. V. Zayats, "All-optical switching in silicon photonic waveguides with an epsilon-near-zero resonant cavity," *Photon. Res.*, vol. 6, no. 5, pp. B1–B5, 2018.
- [2] S. Shang, C. Zhang, H. Zhang, Y. Gao, N. Yi, Q. Song, and S. Xiao, "Enhancing magnetic dipole emission with magnetic metamaterials," *Chin. Opt. Lett.*, vol. 16, no. 5, 2018, Art. no. 050008.
- [3] S. David, V. Jambunathan, A. Lucianetti, and T. Mocek, "Overview of ytterbium based transparent ceramics for diode pumped high energy solid-state lasers," *High Power Laser Sci. Eng.*, vol. 6, no. 4, p. e62, 2018.
- [4] J. Wang, "Metasurfaces enabling structured light manipulation: Advances and perspectives," *Chin. Opt. Lett.*, vol. 16, no. 5, 2018, Art. no. 050006.
- [5] O. Shavit, Y. Ferber, J. Papeer, and E. Schleifer, "Femtosecond laser-induced damage threshold in snow micro-structured targets," *High Power Laser Sci. Eng.*, vol. 6, no. 1, p. e7, 2018.
- [6] Q. Xu, X. Zhang, Y. Xu, C. Ouyang, Y. Li, J. Han, and W. Zhang, "Near-field manipulation of terahertz surface waves by metasurfaces," *Chin. Opt. Lett.*, vol. 16, no. 5, 2018, Art. no. 050002.
- [7] D. Vojna, R. Yasuhara, H. Furuse, O. Slezak, S. Hutchinson, A. Lucianetti, T. Mocek, and M. Cech, "Faraday effect measurements of holmium oxide (Ho_2O_3) ceramics-based magneto-optical materials," *High Power Laser Sci. Eng.*, vol. 6, no. 1, p. e2, 2018.
- [8] R. A. Shelby, D. R. Smith, and S. Schultz, "Experimental verification of a negative index of refraction," *Science*, vol. 292, no. 5514, pp. 77–79, Apr. 2001.
- [9] S. Zhang, W. Fan, K. J. Malloy, S. R. Brueck, N. C. Panoiu, and R. M. Osgood, "Near-infrared double negative metamaterials," *Opt. Express*, vol. 13, no. 13, pp. 4922–4930, 2005.
- [10] O. Paul, C. Imhof, B. Reinhard, R. Zengerle, and R. Beigang, "Negative index bulk metamaterial at terahertz frequencies," *Opt. Express*, vol. 16, no. 9, pp. 6736–6744, 2008.
- [11] J. Valentine, S. Zhang, T. Zentgraf, E. Ulin-Avila, D. A. Genov, G. Bartal, and X. Zhang, "Three-dimensional optical metamaterial with a negative refractive index," *Nature*, vol. 455, no. 7211, pp. 376–379, Aug. 2008.
- [12] R. Maas, J. Parsons, N. Engheta, and A. Polman, "Experimental realization of an epsilon-near-zero metamaterial at visible wavelengths," *Nature Photon.*, vol. 7, no. 11, pp. 907–912, 2013.
- [13] P. A. Belov, A. P. Slobozhanyuk, D. S. Filonov, I. V. Yagupov, P. V. Kapitanova, C. R. Simovski, M. Lapine, and Y. S. Kivshar, "Broadband isotropic μ -near-zero metamaterials," *Appl. Phys. Lett.*, vol. 103, no. 21, Oct. 2013, Art. no. 211903.
- [14] S. M. Mansfield and G. S. Kino, "Solid immersion microscope," *Appl. Phys. Lett.*, vol. 57, no. 24, pp. 2615–2616, Oct. 1990.
- [15] A. Karalis, E. Lidorikis, M. Ibanescu, J. D. Joannopoulos, and M. Soljacic, "Surface-plasmon-assisted guiding of broadband slow and subwavelength light in air," *Phys. Rev. Lett.*, vol. 95, no. 6, Aug. 2005, Art. no. 063901.
- [16] D. F. Sievenpiper, E. Yablonovitch, J. N. Winn, S. Fan, P. R. Villeneuve, and J. D. Joannopoulos, "3D metallo-dielectric photonic crystals with strong capacitive coupling between metallic islands," *Phys. Rev. Lett.*, vol. 80, pp. 2829–2832, Mar. 1998.
- [17] B. Wood and J. B. Pendry, "Metamaterials at zero frequency," *J. Phys. Condens. Matter*, vol. 19, Feb. 2007, Art. no. 076208.
- [18] J. Shin, J.-T. Shen, and S. Fan, "Three-dimensional metamaterials with an ultrahigh effective refractive index over a broad bandwidth," *Phys. Rev. Lett.*, vol. 102, Mar. 2009, Art. no. 093903.
- [19] M. Choi, S. H. Lee, Y. Kim, S. B. Kang, J. Shin, M. H. Kwak, K.-Y. Kang, Y.-H. Lee, N. Park, and B. Min, "A terahertz metamaterial with unnaturally high refractive index," *Nature*, vol. 470, pp. 369–373, Feb. 2011.
- [20] L. Singh, R. Singh, and W. Zhang, "Ultra-high terahertz index in deep subwavelength coupled bi-layer free-standing flexible metamaterials," *J. Appl. Phys.*, vol. 121, no. 23, May 2017, Art. no. 233103.
- [21] I.-S. Lee, I.-B. Sohn, C. Kang, C.-S. Kee, J.-K. Yang, and J. W. Lee, "High refractive index metamaterials using corrugated metallic slots," *Opt. Express*, vol. 25, no. 6, pp. 6365–6371, 2017.
- [22] X. Jing, X. Gui, R. Xia, and Z. Hong, "Ultrabroadband unnaturally high effective refractive index metamaterials in the terahertz region," *IEEE Photon. J.*, vol. 9, no. 1, Feb. 2017, Art. no. 5900107.
- [23] X. Jing, R. Xia, X. Gui, W. Wang, Y. Tian, D. Zhu, and G. Shi, "Design of ultrahigh refractive index metamaterials in the terahertz regime," *Superlattices Microstruct.*, vol. 109, pp. 716–724, Sep. 2017.
- [24] X. Jing, W. Wang, R. Xia, J. Zhao, Y. Tian, and Z. Hong, "Manipulation of dual band ultrahigh index metamaterials in the terahertz region," *Appl. Opt.*, vol. 55, no. 31, pp. 8743–8751, 2016.
- [25] B. Fang, Y. Chen, C. Li, and X. Jing, "Design of multiband isotropic ultrahigh refractive index metamaterials in the terahertz region," *J. Optoelectron. Adv. Mater.*, vol. 20, nos. 7–8, pp. 371–378, Jul. 2018.
- [26] R. Sainidou and F. J. G. de Abajo, "Plasmon guided modes in nanoparticle metamaterials," *Opt. Express*, vol. 16, no. 7, pp. 4499–4506, 2008.
- [27] H. Alaeian and J. A. Dionne, "Plasmon nanoparticle superlattices as optical-frequency magnetic metamaterials," *Opt. Express*, vol. 20, no. 14, pp. 15781–15796, 2012.
- [28] D. R. Smith, D. C. Vier, T. Koschny, and C. M. Soukoulis, "Electromagnetic parameter retrieval from inhomogeneous metamaterials," *Phys. Rev. E, Stat. Phys. Plasmas Fluids Relat. Interdiscip. Top.*, vol. 71, Mar. 2005, Art. no. 036617.

- [29] X. Chen, T. M. Grzegorzczak, B.-I. Wu, J. Pacheco, and J. A. Kong, "Robust method to retrieve the constitutive effective parameters of metamaterials," *Phys. Rev. E, Stat. Phys. Plasmas Fluids Relat. Interdiscip. Top.*, vol. 70, Jul. 2004, Art. no. 016608.
- [30] W. Wang, X. Jing, J. Zhao, Y. Li, and Y. Tian, "Improvement of accuracy of simple methods for design and analysis of a blazed phase grating microstructure," *Opt. Appl.*, vol. 47, no. 2, pp. 183–198, 2017.
- [31] X. Jing, S. Jin, Y. Tian, P. Liang, Q. Dong, and L. Wang, "Analysis of the sinusoidal nanopatterning grating structure," *Opt. Laser Technol.*, vol. 48, no. 6, pp. 160–166, Jun. 2013.
- [32] J. Zhao, X. Jing, W. Wang, Y. Tian, D. Zhu, and G. Shi, "Steady method to retrieve effective electromagnetic parameters of bianisotropic metamaterials at one incident direction in the terahertz region," *Opt. Laser Technol.*, vol. 95, no. 1, pp. 56–62, Oct. 2017.
- [33] S. Lee, S. Kim, T.-T. Kim, Y. Kim, M. Choi, S. H. Lee, J.-Y. Kim, and B. Min, "Reversibly stretchable and tunable terahertz metamaterials with wrinkled layouts," *Adv. Mater.*, vol. 24, no. 26, pp. 3491–3497, Jul. 2012.
- [34] T. H. Taminia, F. D. Stefani, F. B. Segerink, and N. F. Van Hulst, "Optical antennas direct single-molecule emission," *Nature Photon.*, vol. 2, pp. 234–237, Mar. 2008.
- [35] K. B. Alici, A. B. Turhan, C. M. Soukoulis, and E. Ozbay, "Optically thin composite resonant absorber at the near-infrared band: A polarization independent and spectrally broadband configuration," *Opt. Express*, vol. 19, no. 15, pp. 4260–4267, 2011.
- [36] Z. Wang, B. S. Luk'yanchuk, L. Li, P. L. Crouse, Z. Liu, G. Dearden, and K. G. Watkins, "Optical near-field distribution in an asymmetrically illuminated tip-sample system for laser/STM nanopatterning," *Appl. Phys. A, Solids Surf.*, vol. 89, no. 2, pp. 363–368, Nov. 2007.
- [37] M. Kim, S. Lee, J. Lee, D. K. Kim, Y. J. Hwang, G. Lee, G.-R. Yi, and Y. J. Song, "Deterministic assembly of metamolecules by atomic force microscope-enabled manipulation of ultra-smooth, super-spherical gold nanoparticles," *Opt. Express*, vol. 23, no. 10, pp. 12766–12776, 2015.
- [38] D.-K. Kim, Y. J. Hwang, C. Yoon, H.-O. Yoon, K. S. Chang, G. Lee, S. Lee, and G.-R. Yi, "Experimental approach to the fundamental limit of the extinction coefficients of ultra-smooth and highly spherical gold nanoparticles," *Phys. Chem. Chem. Phys.*, vol. 17, no. 32, pp. 20786–20794, 2015.
- [39] C. F. Bohren and D. R. Huffman, *Absorption and Scattering of Light by Small Particles*. Hoboken, NJ, USA: Wiley, 1998.
- [40] A. Yu Akimov, V. P. Olefir, and N. A. Azarenkov, "Influence of azimuthal structure of surface waves on efficiency of their excitation by tubular electron beams," *Contr. Plasma Phys.*, vol. 46, pp. 817–825, Dec. 2006.
- [41] J. T. Shen, P. B. Catrysse, and S. Fan, "Mechanism for designing metallic metamaterials with a high index of refraction," *Phys. Rev. Lett.*, vol. 94, no. 19, p. 197401, 2005.
- [42] A. Pimenov and A. Loidl, "Experimental demonstration of artificial dielectrics with a high index of refraction," *Phys. Rev. B, Condens. Matter*, vol. 74, no. 19, Nov. 2006, Art. no. 193102.
- [43] H. Shi, Y. Lu, X. Wei, X. Dong, and C. Du, "Characterization for metamaterials with a high refractive index formed by periodic stratified metallic wires array," *Appl. Phys. A, Solids Surf.*, vol. 97, no. 4, p. 799, Dec. 2009.
- [44] X. Wei, H. Shi, X. Dong, Y. Lu, and C. Du, "A high refractive index metamaterial at visible frequencies formed by stacked cut-wire plasmonic structures," *Appl. Phys. Lett.*, vol. 97, no. 1, 2010, Art. no. 011904.
- [45] Y. He, S. He, J. Gao, and X. Yang, "Nanoscale metamaterial optical waveguides with ultrahigh refractive indices," *J. Opt. Soc. Amer. B, Opt. Phys.*, vol. 29, no. 9, pp. 2559–2566, 2012.
- [46] Y. H. Teguh, A. P. Tenggara, V. D. Nguyen, T. T. Kim, F. D. Praseetyo, C.-G. Choi, M. Choi, and D. Byun, "Fabrication of terahertz metamaterial with high refractive index using high-resolution electrohydrodynamic jet printing," *Appl. Phys. Lett.*, vol. 103, no. 21, 2013, Art. no. 211106.
- [47] T. Campbell, A. P. Hibbins, J. R. Sambles, and I. R. Hooper, "Broadband and low loss high refractive index metamaterials in the microwave regime," *Appl. Phys. Lett.*, vol. 102, no. 9, 2013, Art. no. 091108.
- [48] S. Tan, F. Yan, L. Singh, W. Cao, N. Xu, X. Hu, R. Singh, M. Wang, and W. Zhang, "Terahertz metasurfaces with a high refractive index enhanced by the strong nearest neighbor coupling," *Opt. Express*, vol. 23, no. 22, pp. 29222–29230, 2015.
- [49] Z. Liu, C. Zhang, S. Sun, N. Yi, Y. Gao, Q. Song, and S. Xiao, "Polarization-independent metamaterial with broad ultrahigh refractive index in terahertz region," *Opt. Mater. Express*, vol. 5, no. 9, pp. 1949–1953, 2015.
- [50] R. Kim, K. Chung, J. Y. Kim, Y. Nam, S. H. K. Park, and J. Shin, "Metal nanoparticle array as a tunable refractive index material over broad visible and infrared wavelengths," *ACS Photon.*, vol. 5, no. 4, pp. 1188–1195, Mar. 2018.



XUFENG JING received the Ph.D. degree from the Shanghai Institute of Optics and Fine Mechanics, Chinese Academy of Sciences (CAS), in 2011. He is currently an Associate Professor of photoelectricity with the College of China Metrology University and a master's tutor. His research interests include nano-photonics, metamaterials, and subwavelength grating fields.



YINUO XU was born in Zhejiang, China. He is currently pursuing the bachelor's degree from China Jiliang University.



HAIYONG GAN is currently an Associate Professor with the National Institute of Metrology, Beijing, China. His research interests include single-photon measurement, metamaterials, and weak light emission standard technology. He is also the Director of the China Optical Engineering Society and a Representative of the Optical Metrology Technical Committee of Asia Pacific Metrology Organization.



YINGWEI HE is currently an Associate Professor with the National Institute of Metrology, Beijing, China. His research interests include single-photon measurement and weak light emission standard technology.



ZHI HONG received the bachelor's and master's degrees from the Department of Electrical Engineering, Zhejiang University, in 1984 and 1987, respectively, and the Ph.D. degree in optical engineering from Zhejiang University, in 2001, where he was a Researcher and a Doctoral Tutor with the Department of Optics, from 1987 to 2005. He was with the Institute of Mechatronics Engineering, China Jiliang University, China, and the Institute of Metrology Terahertz Institute of Technology and Application, Zhejiang University Light. He was an Adjunct Professor and a Doctoral Tutor (currently under the guidance of three doctoral students) with the Electromagnetic Research Center. From 1999 to 2000, he twice went to work at Berkeley in Germany. He was a Visiting Professor with Alberta University, Canada, in 2006. In 2007, he was a Visiting Professor with the Terahertz Research Center, Rennselaer Institute of Technology, USA. He is currently a Research Fellow with the China Institute of Mechatronics Engineering.

...